5-15-1999

Modeling the high-speed switching of far-infrared radiation by photoionization in a semiconductor

Thomas E. Wilson
Marshall University, wilsont@marshall.edu

Modeling the high-speed switching of far-infrared radiation by photoionization in a semiconductor

Thomas E. Wilson*
Department of Physics and Physical Science, Marshall University, Huntington, West Virginia 25755-2570
(Received 24 November 1998; revised manuscript received 16 February 1999)

Data from an earlier study [T. Vogel *et al.*, Appl. Opt. **31**, 329 (1992)] on the subnanosecond switching of 119-μm radiation in high-resistivity silicon by pulsed UV laser radiation, is compared with a refined one-dimensional numerical multilayer model accounting for the generation, recombination, and diffusion of the free carriers on the resulting far-infrared optical properties of the silicon. The inclusion of recent measurements for carrier-density and temperature-dependent transport parameters leads to improved agreement between experiment and theory. [S0163-1829(99)03220-8]

I. INTRODUCTION

The photoexcitation of semiconductors with short laser pulses leads to a rapid change of the free-carrier density if the photon energy exceeds the band-gap energy. The resulting change of the refractive index induces pronounced changes of the transmissivity and reflectivity, particularly in the infrared and the far-infrared (FIR) spectral range. The effect has been used to switch 10-μm CO_2-laser radiation by using a variety of supra-band-gap laser pulses,[2] and to switch FIR laser radiation with subnanosecond risetimes.[3] A number of investigators have also used this method to cavity-dump both free-electron FIR,[4] and optically-pumped, molecular-gas FIR,[5] lasers.

Vogel *et al.*[1] have performed an extensive investigation of the time-dependent FIR reflectivity in photoexcited high-resistivity silicon and compared their results to a one-dimensional multilayer model, which accounted for generation, recombination, and diffusion of the free carriers in the semiconductor wafer. A comparison of their experimental and numerical results showed fair qualitative agreement for the overall temporal behavior of the reflectivity over an interval ranging from 100 ps to 1 ms; the remaining quantitative disagreement was attributed to the lack of a surface recombination mechanism in their numerical simulation. In this paper, we report on a comparison of the experimental reflectivity data of Vogel *et al.* with the numerical results of a refined model. The newer model includes the effect of lattice heating and surface recombination, as well as the density dependence of the diffusivity, the Auger recombination rate, and momentum relaxation rate, via the mobility.

II. PULSED LASER INTERACTION WITH SILICON: CARRIER GENERATION AND HEATING

The absorption of pulsed laser radiation by semiconductors leads to the creation of nonequilibrium carrier densities and elevated carrier and lattice temperatures. The carriers generated by the laser pulse absorption are spatially inhomogeneous due to absorption, diffusion, and lifetime effects. In addition, due to laser heating the material properties may also be spatially inhomogeneous. In the work discussed here we are interested in situations where 10^{-9}-s pulses, with energy densities of mJ/cm^2, interact with the semiconductor. Under these conditions, it is generally acknowledged[6] that the carrier and lattice temperatures are essentially the same. The lattice-carrier temperature may become elevated due to the transfer of the excess energy from recombining electron-hole pairs, as well as by the direct absorption of supra-band-gap laser radiation. If the temperature increase is sufficiently large, a bottleneck can result in the carrier diffusion due to the induced band bending of the semiconductor. Because the band gap of most semiconductors decreases with increasing temperature, the band gap will be lowest near the surface, where the temperature is highest. Brown[7] originally pointed out that this effect could present barriers to the normal diffusion process.

The overall theory for the coupled diffusion of a photoexcited electron-hole plasma and the corresponding lattice-carrier temperature, as per Brown's suggestion, has been thoroughly developed by Gallant *et al.*[8] We summarize the salient features below.

The electron-hole pair current density is written as

$$\vec{J} = -D\left[\vec{\nabla}N + \frac{N}{2T}(1-r)\vec{\nabla}T\right], \tag{1}$$

where D is the ambipolar diffusivity, N is the electron-hole pair density, T is the carrier-lattice temperature, $r = -k_B^{-1}(\partial E_g/\partial T)$, and E_g is the energy gap. A number of assumptions have been made in arriving at Eq. (1); these are: (1) the carrier distributions are nondegenerate, (2) the carrier scattering times are determined solely by carrier-phonon interactions, (3) a particular choice for the energy dependence of the carrier-phonon scattering has been used, and (4) the spatial variation of the band gap is due to variation of the lattice temperature only. The evolution of the carrier density can then be determined through the equation of continuity, which is given by

$$\frac{\partial N}{\partial t} + \vec{\nabla}\cdot\vec{J} = \frac{(1-R)\alpha I(t)}{\hbar\omega}\exp(-\alpha z) - \gamma_3 N^3 - \gamma_2 N^2 - \gamma_1 N, \tag{2}$$

where it has been assumed that the pairs are generated at a depth z through band-to-band absorption by a single pulse of intensity $I(t)$ and photon energy $\hbar\omega$ incident on the semiconductor at an angle with an associated reflectivity R and absorption coefficient α. In the experiment of Vogel *et al.*,

TABLE I. Material properties for silicon.

R (337 nm, $\theta=26°$)	0.60	1
α	$1.0\times10^{6}(1.+T/2000)$ cm^{-1}	9
K_T	$1585T^{-1.23}$ W/cmK	9
C	$1.978+(3.54\times10^{-4})T-(3.68)T^{-2}$ J/cm^2 K	9
r	3.25	17
γ_1^*	2×10^{5} s^{-1}	1
γ_2	5×10^{-14} cm^3/s	1
γ_3^*	3.8×10^{-31} cm^{6}s^{-1}	1
D^*	17.9 cm^2/s	1

the UV photon energy is 3.68 eV, which exceeds the indirect energy gap (1.11 eV); hence, strong absorption (10^6 cm^{-1}) occurs near the semiconductor surface. The bulk carrier recombination consists of three components: Auger recombination, radiative recombination, and recombination via lattice imperfections and impurities. These components are characterized by coefficients γ_3, γ_2, and γ_1, respectively. As discussed below, γ_3 has recently been shown to be a function of the injected carrier density and temperature.

Equations (1) and (2) can be combined to give the density diffusion equation

$$\frac{\partial N}{\partial t}=\vec{\nabla}\cdot D\left[\vec{\nabla}N+\frac{N}{2T}(1-r)\vec{\nabla}T\right]+\frac{(1-R)\alpha I(t)}{\hbar\omega}\times\exp(-\alpha z)-\gamma_3(N,T)N^3-\gamma_2N^2-\gamma_1N. \quad (3)$$

Equation (3) must be solved in the one dimensional approximation subject to the boundary conditions

$$N(z=L,t)=N_i$$

$$D\left(\frac{\partial N}{\partial z}\right)_{z=0}=S(N-N_i), \quad (4)$$

where L is the sample thickness, $N_i\simeq10^{12}/\text{cm}^3$ is the intrinsic equilibrium carrier density appropriate to high-resistivity silicon and S is the surface recombination velocity, which depends upon surface conditions. The value of S ranges from $\sim10^2$ cm/s for polished and chemically etched surfaces to $\sim10^6$ cm/s for mechanically polished surfaces. A one-dimensional approximation is justified, at least in the initial phase, because the absorption depth of the UV radiation (10^{-5} mm), and hence the layer in which the free carriers are created, is small compared with the diameter (1.6 mm) of the homogeneously irradiated area.

In general, because of the lattice-temperature dependence of the material parameters and the $\vec{\nabla}T$ term, Eq. (3) must be solved self consistently with an equation, which describes the evolution of the carrier-lattice temperature. It will be assumed that the electron-hole pairs instantaneously lose their excess energy $[\hbar\omega-E_g-2(\frac{3}{2}k_BT)]$, imparted to them in the absorption process, so that the effective heat generation depth is α^{-1}. The thermal diffusion equation can therefore be written in the form

$$\frac{\partial T}{\partial t}=\frac{\partial}{\partial x}\left(D_L\frac{\partial T}{\partial x}\right)+\frac{(1-R)I(t)\alpha e^{-\alpha x}}{C}(\hbar\omega-E_g-3k_BT)+\frac{(E_g+3k_BT)}{C}(\gamma_3N^3+\gamma_2N^2+\gamma_1N), \quad (5)$$

where C is the specific heat and D_L is the lattice thermal diffusivity. Heat generation occurs via the bulk recombination processes in which the energy $E_g+2(\frac{3}{2}k_BT)$ lost by the recombining electron-hole pair is transferred immediately to the lattice. On a nanosecond time scale little heat is lost from the surface. On the other hand, heat is generated at the surface if the surface recombination velocity is different from zero. Equation (5) must therefore be solved subject to the boundary conditions

$$K_T\frac{\partial T}{\partial x}+S(N-N_i)(E_g+3k_BT)=0$$

$$T(z=L)=300 \text{ K}, \quad (6)$$

where K_T (and $D_L=K_T/C\simeq0.683$ cm^2/s) is the thermal conductivity. The values of the material parameters and their temperature dependence for $300<T<1000$ K are given in Table I. (An associated asterisk implies either a carrier density and/or a sample dependence.)

The laser intensity, assuming a sine-square-shaped laser pulse, can be written as

$$I(t)=\begin{cases}\dfrac{E}{\delta A}\sin^2\left(\dfrac{\pi t}{2\delta}\right) & \text{for } 0\leq t\leq2\delta\\ 0 & \text{otherwise}\end{cases} \quad (7)$$

where E is the integrated pulse energy, δ is the (FWHM) pulsewidth, and A is the irradiated area. In the experiments of Vogel *et al.*, these were 30 μJ, 1.7 ns, and 2.0×10^{-2} cm^2, respectively.

The coupled, nonlinear diffusion Eqs. (3)–(6) have been numerically solved[10] using the FORTRAN DMOLCH routine of the IMSL program library (IMSL, Houston, TX). We have also[1] approximated the semiconductor sample of thickness $L=436$ μm by a series of $q=1500$ homogeneous sublayers. The thickness of the sublayers was varied between 0.3 nm on the optically-excited side of the sample and 2.6 on the opposite side according to the following relation

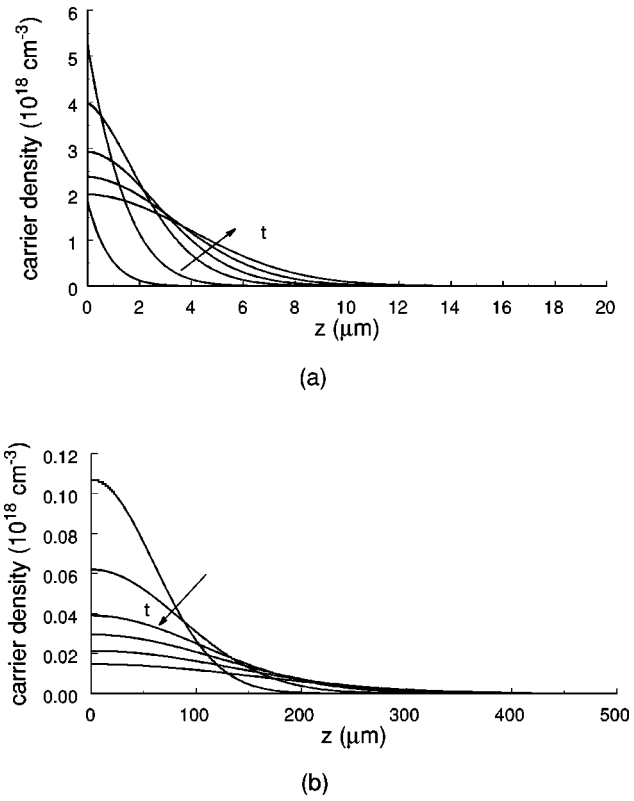

FIG. 1. Time-dependent evolution of the carrier density profile in Si after UV excitation. (a) Six equidistant time steps from 1 to 6 ns. (b) Six equidistant time steps from 1 to 6 microseconds.

$$z_i = c\{\exp[(i-1)/(n-1)\ln(L/c+1)]-1\}, \qquad (8)$$

where z_i is the position of the boundary between sublayers i and $i-1$ and c is a constant, here equal to 0.05 μm. The number of resulting sublayers within the UV penetration depth ($\alpha^{-1}=10^{-6}$ cm) is $\simeq 30$. An increase in the number of sublayers did not cause any significant change in the results.

Figure 1 shows the carrier-density profiles which occur at different times during, and after, UV excitation for the case of $S=0$ and using the same constant transport parameters as Vogel *et al.* The maximum of the carrier density, which occurs at nearly the same time as the maximum UV power, is approximately 5×10^{18} cm^{-3}. The profiles are in agreement with the simulated profiles depicted in Fig. 1 of Vogel *et al.;* unfortunately, there are no experimental profiles for comparison.

The calculated temperature profile, which is not shown, only rises 5.19 K above the ambient temperature (300 K) at the surface and this maximum occurs near the time for which the laser power is near its maximum. The small rise in temperature can be explained as follows. Due to thermal diffusion, over the time of laser excitation ($2\delta=3.4$ ns) the laser energy ($E=30$ mJ) spreads throughout a depth ($d \sim \sqrt{2D_L 2\delta}=6.8\times10^{-5}$ cm) much larger than the absorption depth ($\alpha^{-1}=10^{-6}$ cm). As a result, the surface temperature increase is rather small, i.e., an estimate for the average temperature increase throughout the volume is given by $(1-R)E/(AdC)\sim 4$ K, in good agreement with the calculated rise.

We have also calculated the carrier density profiles (not shown) in the presence of surface recombination for values up to 10^4 cm/s. For early times ($\leqslant 10$ ns), the presence of surface recombination alters the carrier density profiles only slightly; however, after some microseconds, a pronounced reduction in the carrier density at the surface is observed. Similarly, the maximum surface temperature with this level of surface recombination is only slightly higher than that calculated in the case of no surface recombination and constant diffusivity, i.e., 305.21 K compared to 305.19 K. Although we initially had suspected otherwise, for the experiments under consideration, the very slight heating effects from both the laser radiation absorption and carrier recombination processes do not appear to create any barrier to the normal diffusion process due to thermally-induced band bending.

In an effort to improve the model, we have also considered the following. Auger recombination is well known to influence the characteristics of semiconductor devices at high-injection levels (below some 10^{18} cm^{-3}), and the specific dependence of the Auger band-to-band recombination on the carrier density and temperature is an active area of research. For these reasons, the use of a constant γ_3 in Eqs. (3)–(4) is not valid. We use the functional dependence proposed by Jonsson *et al.*[11] in which the Auger coefficient is taken to consist of two parts: the *e-e-h* Auger coefficient C_n and the *e-h-h* coefficient C_p, i.e.,

$$\gamma_3(N,T)=\begin{cases} C_n+C_p \ \ (\mathrm{cm}^6/\mathrm{s}) \\ C_n=2.8\times10^{-31}(T/300)^{0.6}+[5.3\times10^{-31}\times(T/300)^{2.27}]/\{1+[N/(2\times10^{18})]^2\} \\ C_p=0.99\times10^{-31}(T/300)^{0.6}+[1.9\times10^{-31}\times(T/300)^{2.27}]/\{1+[N/(2\times10^{18})]^2\}. \end{cases}$$

Another questionable assumption used in the solution of the carrier profiles shown in Fig. 1 was that of a constant diffusivity. In undoped silicon, measurements extracted from transient grating experiments[12] show that the effective ambipolar diffusivity is a function of injected carrier density. The diffusivity is reduced from the value 17.9 cm^2/s obtained by using constant electron and hole diffusivities. The reduction occurs for carrier concentrations exceeding 10^{15} cm^{-3} and reaches a minimum of ≈ 9 cm^2/s near $\sim 10^{18}$ cm^{-3}. At even higher densities (typically above 10^{19} cm^{-3} for $T \leqslant 300$°C) degeneracy will occur and the diffusion coefficient increases steeply with carrier concentration, due mainly to an increase in the kinetic energy of the carriers. We therefore have used a functional dependence of the ambipolar diffusivity upon the carrier density, $D(N)$, obtained from a logarithmic fit to data published by Linnros and Grivickas.[13]

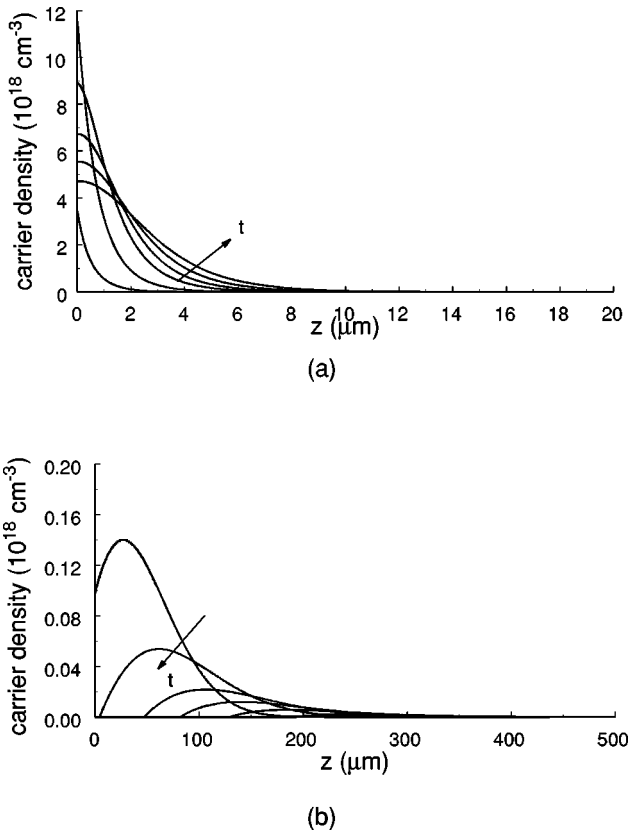

FIG. 2. Time-dependent evolution of the carrier density profile in Si after UV excitation for nonconstant transport parameters and $S=10^3$ cm/s. (a) Six equidistant time steps from 1 to 6 ns. (b) Six equidistant time steps from 1 to 6 μm.

Figure 2 shows the numerical profiles that result from the density-dependent characterizations of the Auger band-to-band recombination and ambipolar diffusivity. The smaller nonconstant diffusivity results in higher injected carrier densities at the surface ($\sim 2x$), compared to those of Fig. 1. At later times, one notices the effects, as described above, of an incorporated surface recombination velocity of $S=1\times 10^3$ cm/s. For instance, the peak carrier densities have migrated away from the surface, although the peak values remain of the same order of magnitude as those at the surface in the case of no surface recombination. Also, the maximum calculated surface temperature is again only slightly higher than that calculated in the case of no surface recombination and constant diffusivity.

III. COMPLEX DIELECTRIC CONSTANT

The Drude model[14] treats the free carriers in a solid as classical point charges subject to random collisions. The simplest version of the Drude model is adopted in which the collision damping is independent of the carrier energy. The linear interaction between an isotropic medium and electromagnetic radiation is, in general, described by a frequency-dependent complex dielectric constant $\boldsymbol{\varepsilon}(\omega)$, being the square of the complex refractive index $\mathbf{n}=n_R+in_I$. Furthermore, when the medium is anisotropic, both the dielectric constant and refractive index are space dependent. The Drude model has been successfully used to model the minimum in the infrared reflectivity of photoexcited silicon as a function of the laser fluence,[15] and to model the index of refraction as a function of FIR frequency in extrinsically doped silicon; although in the latter case an extended Drude model with an energy-dependent carrier-relaxation rate was necessary.[16] Other than the work of Vogel *et al.*,[1] we know of no experimental study for which measurements of the FIR reflectivity of photoexcited silicon, as a function of the delay time from the excitation laser pulse, have been published. According to the Drude model for a plasma with equal numbers of electrons and hole, the dielectric constant in SI units is

$$\varepsilon=\varepsilon_\infty+\frac{i\sigma}{\omega\varepsilon_0}=\varepsilon_\infty-\frac{\omega_{pe}^2}{\omega(\omega+i\Gamma_e)}-\frac{\omega_{ph}^2}{\omega(\omega+i\Gamma_h)}, \quad (9)$$

where $\varepsilon_\infty=11.7$ is the contribution of the dielectric and the parameter indices e and h refer to electrons and holes, respectively. $\Gamma_{e/h}=1/\tau_{e/h}$ is the damping rate with $\tau_{e/h}$ the average collision time. The plasma angular frequency $\omega_{p(e/h)}$ is defined by $\omega_{p(e/h)}^2=Ne^2/\varepsilon_0 m_{e/h}$, where N is the carrier density, e is the electronic charge, ε_0 is the free-space permittivity, and $m_{e/h}$ is the effective carrier mass. The damping rate $\Gamma_{e/h}$ is obtained from the mobility by $\Gamma_{e/h}=e/(m_{e/h}\mu_{e/h})$. For silicon, $m_e=0.26m_0$ and $m_h=0.37m_0$.[16] Vogel[1] used the constant mobility values[17] $\mu_e=1350$ cm^2/(V s) and $\mu_e=480$ cm^2/(V s). We have also included the density dependence of the ambipolar mobility, which can be obtained from the ambipolar diffusivity by the Einstein relation $D=kT/e\mu$. The density-dependent values were obtained by scaling the diffusivity data of Linnros and Grivickas.[13] The electron and hole mobilities become equal to the ambipolar mobility for carrier densities above 10^{14} cm^{-3}. (However, the extraction of the scattering times of electron/holes from the ambipolar mobility may be an oversimplified approach and not justifiable. In addition, for carrier densities greater than 5×10^{17} cm^{-3} (the Mott transition in silicon), an extrapolation from the Brooks-Herring mobility formula ought to be used as the Einstein relation is not valid.[18] These objections may be more fully addressed in future work.)

The real and imaginary parts of the complex refractive index, as functions of the real and imaginary parts of the complex dielectric function, are given by

$$2n_R^2=\varepsilon_R+(\varepsilon_R^2+\varepsilon_I^2)^{1/2}$$

$$2n_I^2=-\varepsilon_R+(\varepsilon_R^2+\varepsilon_I^2)^{1/2} \quad (10)$$

In Fig. 3, we display the real (n_R) and imaginary (n_I) parts of the refractive index as calculated from the carrier density profiles of Fig. 2 where we have used density-dependent mobilities. The maximum surface value for the real part of the refractive index is nearly doubled (10.6 versus 5.9) compared to that (not shown) associated with the carrier density profiles of Fig. 1. On the other hand, the maximum surface value of the imaginary part of the refractive index is reduced – a value of approximately 16 compared to nearly 20 in the case of the carrier density profiles of Fig. 1.

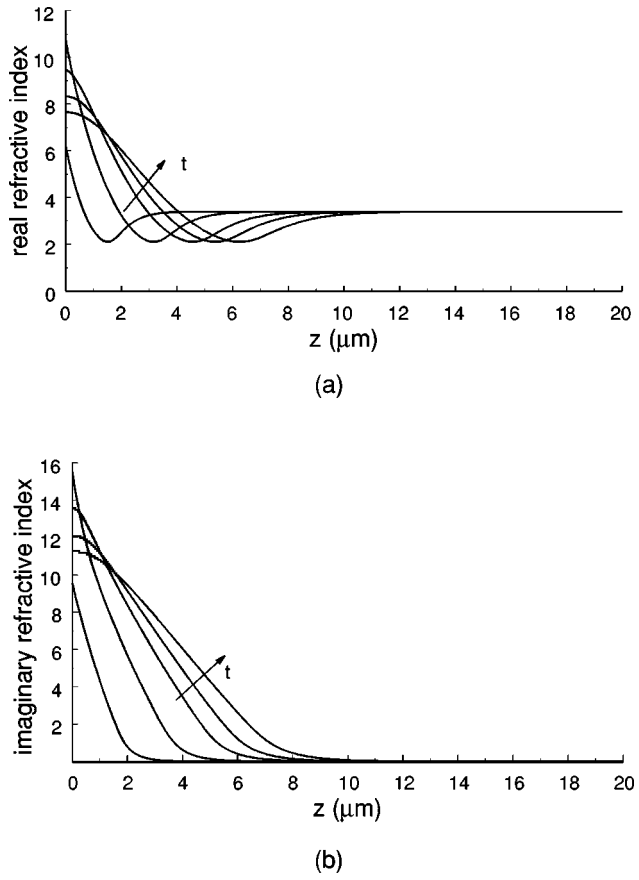

FIG. 3. Time-dependent evolution of the index of refraction in Si after UV excitation for five equidistant time steps from 1 to 5 ns as calculated from the data in Fig. 2. (a) real part (b) imaginary part.

IV. CHARACTERISTIC MATRIX METHOD AND REFLECTIVITY

The reflectivity of optically absorbing inhomogeneous materials can be treated using the characteristic matrix method for stratified media.[19] If the so-called characteristic matrix $\mathbf{M}(z)$ of a stratified medium is known, the propagation of a plane wave in the medium can be calculated. In this context, one approximates the inhomogeneous one-dimensional layer, as a strata of q homogeneous sublayers [as per Eq. (8)] of individual thicknesses $\Delta z_k = z_{k+1} - z_k$, $k = 1,2,\ldots q$. The inhomogeneous layer itself extends from $z_1 = 0$ to $z = z_{q+1}$ and is bounded on each side by a homogeneous semi-infinite medium (air in our case). The complex coefficients $\mathbf{r}$ and $\mathbf{t}$ of reflection and transmission are then given by

$$\mathbf{r} = \frac{(\mathbf{m}_{11} + \mathbf{m}_{12}\mathbf{p}_{q+2})\mathbf{p}_1 - (\mathbf{m}_{21} + \mathbf{m}_{22}\mathbf{p}_{q+2})}{(\mathbf{m}_{11} + \mathbf{m}_{12}\mathbf{p}_{q+2})\mathbf{p}_1 + (\mathbf{m}_{21} + \mathbf{m}_{22}\mathbf{p}_{q+2})} \tag{11}$$

$$\mathbf{t} = \frac{2\mathbf{p}_1}{(\mathbf{m}_{11} + \mathbf{m}_{12}\mathbf{p}_{q+2})\mathbf{p}_1 + (\mathbf{m}_{21} + \mathbf{m}_{22}\mathbf{p}_{q+2})}. \tag{12}$$

The complex quantities $\mathbf{m}_{ij}$ $(i,j = 1,2)$ are the elements of the characteristic matrix taken at $z = z_{q+1}$. In the particular case when the magnetic-field vector is perpendicular to the plane of incidence (TM wave), corresponding to the experimental arrangement of Vogel *et al.*, the complex quantities $\mathbf{p}_k$ and $\mathbf{v}_k$ (needed below) are defined by

$$\mathbf{p}_k = \sqrt{\frac{\varepsilon_k}{\mu_k}}\cos\theta_k = \frac{\mathbf{n}_k}{\mu_k}\cos\theta_k \tag{13}$$

$$\mathbf{v}_k = \sqrt{\frac{\mu_k}{\varepsilon_k}}\cos\theta_k = \frac{\sqrt{\mu_k}}{\mathbf{n}_k}\cos\theta_k . \tag{14}$$

Here, ε_1 (and ε_{q+2}) and μ_1 (and μ_{q+2}) are the complex dielectric constant and the relative permeability of the first (and last) bounding medium and θ_1 (and θ_{q+2}) is the complex angle between the direction of propagation and the z direction in the first (and last) medium. The characteristic matrix $\mathbf{M}_k$ of the kth homogeneous sublayer is given by

$$\mathbf{M}_k = \begin{pmatrix} \cos(k_0\mathbf{p}_{k+1}\Delta z_k) & \dfrac{-i}{\mathbf{v}_{k+1}}\sin(k_0\mathbf{p}_{k+1}\Delta z_k) \\ -i\mathbf{v}_{k+1}\sin(k_0\mathbf{p}_{k+1}\Delta z_k) & \cos(k_0\mathbf{p}_{k+1}\Delta z_k) \end{pmatrix}, \tag{15}$$

where k_0 is the wave number $2\pi/\lambda_0$ of the FIR radiation of vacuum wavelength λ_0. The overall characteristic matrix of the inhomogeneous layer is then given by

$$\mathbf{M}(z_{q+1}) = \prod_{k=1}^{q} \mathbf{M}_k . \tag{16}$$

In order to perform the matrix multiplication of Eq. (16), one first needs the $\mathbf{p}_k$ and $\mathbf{v}_k$; these may be obtained from a backward recursion resulting from a complex form of Snell's law of refraction applied across the sublayers, i.e.,

$$\mathbf{v}_k = \sqrt{1/\mathbf{n}_k^2 - (\mathbf{n}_{k+1}/\mathbf{n}_k)^4(1/\mathbf{n}_{k+1}^2 - \mathbf{v}_{k+1}^2)} \tag{17}$$

$$\mathbf{p}_k = \mathbf{n}_k^2\mathbf{v}_k . \tag{18}$$

The starting quantities $\mathbf{v}_{q+2}$ and $\mathbf{p}_{q+2}$ (which also are equal to $\mathbf{v}_1$ and $\mathbf{p}_1$, respectively) are determined by ε_1 and $\mu_1 = 1$ of the first bounding nonmagnetic medium (air), and the real angle of incidence of the TM FIR radiation. Finally, the reflectivity $\mathcal{R}$ and the transmissivity $\mathcal{T}$ are determined by

$$\mathcal{R} = |\mathbf{r}|^2; \quad \mathcal{T} = \frac{\mathbf{p}_{q+2}}{\mathbf{p}_1}|\mathbf{t}|^2. \tag{19}$$

V. COMPARISON OF THE EXPERIMENTAL AND THEORETICAL RESULTS

In Fig. 4, we show the calculated reflectivity for the case of constant transport parameters for a number of successively increasing values of the surface recombination velocity. Shown for comparison is the experimental data which was scanned from the original publication. Although fair qualitative agreement is seen [the case of $S = 0$ cm/s is identical to that of Fig. 11(a) of Vogel *et al.*, the inclusion of recombination does not significantly improve the agreement. The simulations show a more narrow secondary reflectivity feature than the data for long delay time. One also notes that the maximum for the calculated reflectivity is more than 10% larger and decays more rapidly during the first 10 nanoseconds, than the experimental data.

Figure 5 displays the reflectivity profiles calculated using the density-dependent transport properties discussed above. Although the long-time behavior is not improved, the maxi-

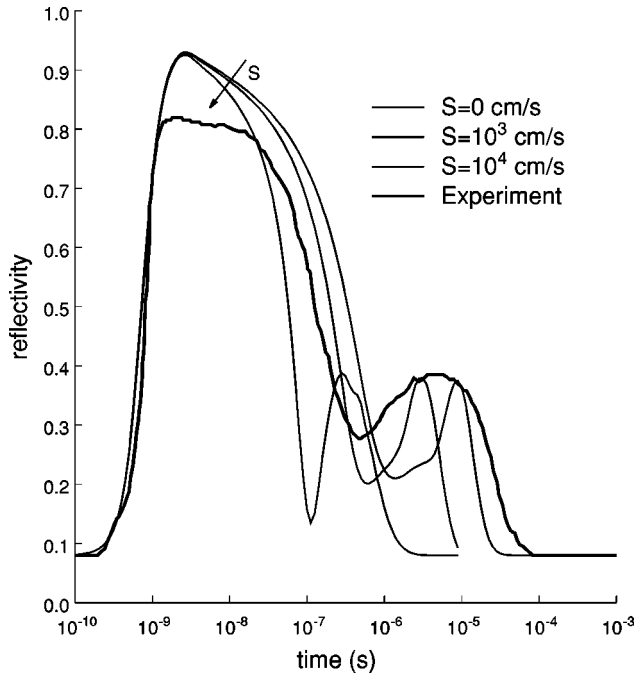

FIG. 4. Reflectivity using constant transport parameters for a variety of *S* values.

mum simulated reflectivity (84%) is much closer to the experimental value (82%) and this agreement is not substantially altered for the values of the surface recombination listed. Also one notices a slower decay during the first 10 ns compared to Fig. 4, which is in better agreement with the data. However, compared to Fig. 4, the reduced diffusivity leads to somewhat higher values of the reflectivity in the time region of 100-1000 ns for similar surface recombination values and thus poorer agreement with experiment for these delay times.

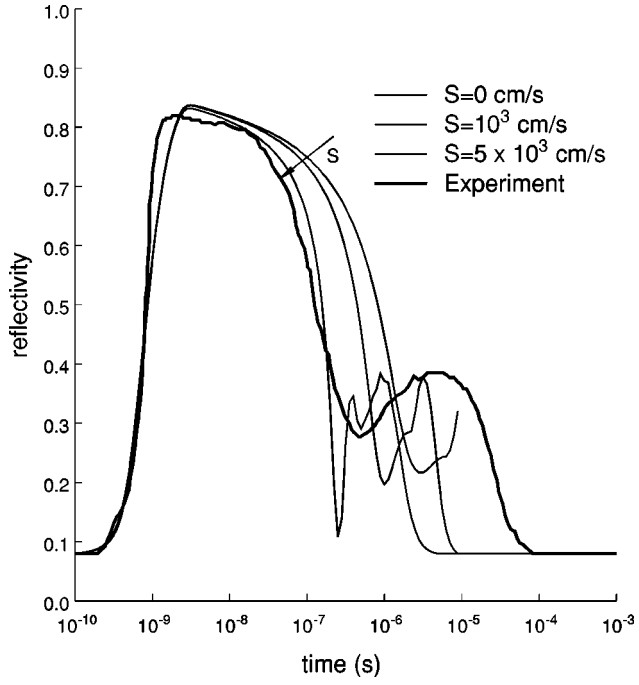

FIG. 5. Reflectivity using carrier density-dependent transport parameters for a variety of *S* values.

In addition, it was found that if the UV pulsewidth in the simulation was decreased while maintaining constant pulse energy, that the rise in reflectivity (not shown) began earlier but that the peak in the reflectivity still occurred at the same time as the simulations shown in Figs. 4-5, i.e., near 3 ns.

The simulations shown both in Fig. 4 and in Fig. 5 have assumed that the front and rear sample faces are parallel; in the experiment, the sample faces were wedged. An attempt was made to account for the variation (2 microns) in the actual sample thickness over the diameter of the FIR beam. The FIR beam is able to penetrate to the rear face only in the case of small plasma density; therefore, it will be assumed that with negligible error, one can average the computed reflectivity over a large number of samples (100 in our case), each of which differing only from the next thinnest sample by the addition of a silicon slice of thickness of 0.02 microns and intrinsic silicon dielectric constant, placed onto the rear of the sample. The range in thicknesses was adjusted so that the average was equal to the actual sample thickness under consideration (436 microns). The resultant time-dependent FIR reflectivity averaged over 100 such samples was not noticeably different from that resulting from a calculation employing only a single sample thickness and is not shown.

VI. SUMMARY

In an effort to obtain better agreement with measurements by Vogel *et al.*[1] of the time-dependent far-infrared reflectivity of silicon, we have performed numerical simulations of (1) the time and space dependencies of the photoexcited electron-hole carrier densities and carrier-lattice temperature, (2) the corresponding time and space dependencies of the real and imaginary parts of the far-infrared index of refraction and finally, (3) the resulting time-dependent far-infrared reflectivity.

Since it is possible[8] for a bottleneck in carrier diffusion, resulting from the induced band-bending of the semiconductor, to occur in the presence of a sufficiently severe temperature inhomogeneity, we have investigated whether such an effect may have been present in the data of Vogel *et al.* We have therefore simultaneously solved coupled nonlinear diffusion equations for the carrier density and the carrier-lattice temperature, also taking into account carrier recombination as a boundary condition at the photoexcited surface. That the temperature distribution would peak at the surface is clear–a result of the heat released by the excess energy of pair creation in the thin UV laser radiation absorption layer according to Beer's law, as well as by the heat generated at the imperfect surface by carrier recombination. Simulation has shown, however, that the temperature inhomogeneity is far too mild to pose any obstacle to carrier diffusion. Also, as Fig. 4 illustrates, the added effect of surface recombination by itself does not lead to any substantial improvement in the level of agreement between simulation and data.

We have also used recent measurements of the carrier-density dependence of both the carrier diffusivity[13] and the Auger recombination coefficient,[11] in Eqs. (3) and (4). The resulting decrease in the diffusivity with high-carrier density leads to approximately a factor of two increase in the peaks of the carrier density profiles for early (1-10 ns) times. We can state also with some confidence that, over the range of

carrier densities considered, the carrier-dependent diffusivity more strongly affects the FIR reflectivity profile than the carrier-dependent Auger recombination coefficient.

Furthermore, we have also incorporated the density dependence of the mobilities (from the density-dependent diffusivity via the Einstein relationship) in the expressions for the complex index of refraction and dielectric constant. In particular, we find that the decrease in the carrier mobility with large carrier density is the primary reason for the closer agreement between simulation and data for: (1) the calculated FIR reflectivity maximum (84% and 82%, respectively), and (2) the time decay of the FIR reflectivity in the time interval from 1-10 ns. Otherwise, the refinements in the model do not lead to substantial quantitative improvement. In particular, the secondary peak in the reflectivity is much broader than the calculations predict. Also, we note that a calculation of the FIR reflectivity averaged over a large number of samples of slightly varying thicknesses, adjusted so that the average thickness equals that of the actual sample, does not differ noticeably from the reflectivity resulting from a calculation using only a single sample.

ACKNOWLEDGMENTS

We wish to acknowledge the able assistance of Jiang Ying, and the generous support of the Army Research Office under Grant No. DAAH04-96-1-0401. The FORTRAN file is available upon request.

*Electronic address: wilsont@marshall.edu

[1] T. Vogel, G. Dodel, E. Holzhauer, H. Salzmann, and A. Theurer, Appl. Opt. **31**, 329 (1992).

[2] A. J. Alcock, P. B. Corkum, and D. J. James, Appl. Phys. Lett. **27**, 680 (1975).

[3] H. Salzmann, T. Vogel, and G. Dodel, Opt. Commun. **47**, 340 (1983); W. M. Dennis, J. Opt. Soc. Am. B **6**, 1045 (1989); J. Burghoorn, J. P. Kaminski, R. C. Strijbos, T. O. Klaassen, and W. Th. Wenckebach, *ibid.* **9**, 1888 (1992).

[4] J. P. Kaminski, J. S. Spector, C. L. Felix, D. P. Enyeart, D. T. White, and G. Ramian, Appl. Phys. Lett. **57**, 2770 (1990).

[5] T. E. Wilson, Bull. Am. Phys. Soc. **32**, 328 (1987); R. E. M. de Bekker, L. M. Claessen, and P. Wyder, J. Appl. Phys. **68**, 3729 (1990); T. E. Wilson, in *Proceedings of the International Conference on Lasers '91*, edited by F. J. Duarte and D. G. Harris (STS Press, McLean, VA, 1992), pp. 762–767; Int. J. Infrared Millim. Waves **14**, 303 (1993).

[6] P. C. Hein, M. I. Gallant, and H. M. van Driel, Solid State Commun. **39**, 601 (1981).

[7] W. L. Brown, in *Laser and Electron Beam Processing of Materials*, edited by C. W. White and P. S. Peercy (Academic, New York, 1980), p. 22.

[8] M. I. Gallant and H. M. van Driel, Phys. Rev. B **26**, 2133 (1982).

[9] Henry M. van Driel, Phys. Rev. B **35**, 8166 (1986).

[10] This double-precision routine was executed on a Pentium Pro 200 workstation running Digital Equipment Corporation (Maynard, MA) VISUAL FORTRAN under Microsoft (Seattle, WA) Windows NT 4.0. Execution times ranged from less than several hours ($S=0$ cm/s) to several weeks ($S=5\times10^4$ cm/s). It must be noted that the routine requires the time derivative of the boundary conditions and that recommended values of the parameters TOL and HINIT are DSQRT[DMACH(4)] and 0.1*TOL, respectively.

[11] P. Jonsson, H. Bleichner, M. Isberg, and E. Nordlander, J. Appl. Phys. **81**, 2256 (1997).

[12] V. Grivickas, J. Linnros, A. Galeckas, and V. Bikbajevas, *Proceedings of the 23rd International Conference on the Physics of Semiconductors* (World Scientific, Singapore, 1996), p. 91.

[13] Jan Linnros and Vytautas Grivickas, Phys. Rev. B **50**, 16 943 (1994). See also Chun-Mao Li, Theodore Sjodin, and Hai-Lung Dai, *ibid.* **56**, 15 252 (1997); M. Rosling, H. Bleichner, P. Jonsson, and E. Nordlander, J. Appl. Phys. **76**, 2855 (1994).

[14] N. W. Ashcroft and N. D. Mermin, *Solid State Physics* (Holt, Rinehart, and Winston, New York, 1976).

[15] J. S. Preston and H. M. van Driel, Phys. Rev. B **30**, 1950 (1984).

[16] Martin van Exter and D. Grischkowsky, Phys. Rev. B **41**, 12 140 (1990).

[17] *Semiconductors: Physics of Group IV Elements and III-V Compounds*, edited by K. H. Hellwege, Landolt-Bornstein Numerical Data and Functional Relationships in Science and Technology (Springer-Verlag, Berlin, 1982), p. 387.

[18] Vytautas Grivickas (private communication).

[19] M. Born and E. Wolf, *Principles of Optics*, 6th ed. (Pergamon, New York, 1980), pp. 55 and 627.